Icarus 383 (2022) 115084

Contents lists available at ScienceDirect

Icarus

journal homepage: www.elsevier.com/locate/icarus

Average VNIR reflectance: A rapid, sample-free method to estimate glass content and crystallinity of fresh basaltic lava

E. Rader [a,*], S. Ackiss [a], A. Sehlke [b], J. Bishop [c], B. Orrill [d], K. Odegaard [a], M. Meier [a], A. Doloughan [a,e]

[a] University of Idaho, Department of Geological Sciences, Moscow, ID 83844, USA
[b] NASA Ames Research Center/ Bay Area Environmental Research Institute, Moffett Field, CA 94035, USA
[c] SETI Institute, Moutain View, CA, USA
[d] Arizona State University, Tempe, AZ, USA
[e] Terracon, Olathe, KS, USA

ARTICLE INFO

Keywords:
In-situ analysis
Planetary exploration

ABSTRACT

The microcrystalline texture in basaltic lava, scoria, and spatter can vary widely from pure glass to holocrystalline due to complex cooling histories after eruption. How quickly a molten rock cools is a function of the environmental surroundings, including water, ice, sustained heat source, and atmospheric conditions. Thus, petrologic texture serves as an indicator of cooling history captured in the rock record. As basalt is a common component of terrestrial bodies across the solar system, relating the abundance of crystalline components to spectral character would allow for a more thorough understanding of the cooling history and emplacement conditions on planetary surfaces. Visible/near-infrared (VNIR) reflectance spectroscopy has been used to examine the absorptions associated with volcanic glass, however, the non-linearity of absorption features in this spectral region requires complex spectral unmixing modeling to achieve modal percentages of minerals. Here we present evidence that average reflectance from 500 to 1000 nm (referred to as $R_{500–1000}$) of solid surface samples is indicative of the crystal texture and degree of glassiness of basaltic rocks. Several factors, such as sample surface roughness, lichen cover, coatings, weathering, and chemical composition can affect the $R_{500–1000}$ of a sample. However, our data indicate that these factors can be sufficiently controlled during sample selection to attribute relative glassiness values to basaltic surfaces. This quick and straightforward method requires no sample preparation or modeling and is demonstrated with training data from sixteen rocks from five basaltic flow fields with differing mineralogy, surface qualities, and geochemistry across Idaho and Oregon, USA. We further test our relationship with two published datasets of synthetic and natural basalts, as well as a subset of our own data collected with our methods to examine the sensitivities of the correlation. This method has the potential to broadly identify glassier basaltic lavas across planetary surfaces. This could be applied toward understanding lava eruption temperatures, cooling rates, magma petrogenesis, paleoclimate reconstruction, and astrobiology due to the involvement of water in quenching of lava.

1. Introduction

1.1. The importance of bulk crystallinity

The crystal content and crystal texture of a volcanic rock provide information about the cooling history of the lava (e.g., DeGraff et al., 1989; Burkhard, 2002; Armienti, 2008; Bernard and de Maisonneuve, 2020). Cooling and crystallization occur in the magma chamber, during magma ascent, and also during surface emplacement. The cooling rate may result in distinct microcrystalline textures and surface morphologies (Griffiths, 2000; Wall et al., 2014; Biren et al., 2020). Two main factors that contribute to the cooling of volcanic rock ascending from the (shallow) magma chamber include interaction with ice or water (e.g., Pupier et al., 2008), and surface cooling as lava flows further from the vent (e.g., Cashman et al., 1999; Robert et al., 2014). X-ray diffraction (XRD) results of explosive basaltic products (ash, cinder, scoria) from numerous basaltic systems around the planet have shown that the petrology and crystallinity can be related to the cooling rate during

* Corresponding author.
E-mail address: erader@uidaho.edu (E. Rader).

https://doi.org/10.1016/j.icarus.2022.115084
Received 9 December 2021; Received in revised form 5 May 2022; Accepted 9 May 2022
Available online 15 May 2022

eruption, which in turn, is linked to the interaction of magma and water during or shortly before eruption (Wall et al., 2014; McBride et al., 2019). Therefore, segments of a basaltic lava flow with high proportions of glass relative to mineral crystals are a result of faster cooling and are associated with water-lava interactions (Mastin, 2007; Gregg and Fornari, 1998; Keszthelyi and Denlinger, 1996). Knowing bulk crystallinity is also an important factor in lava flow modeling and forecasting of eruption dynamics (Woitischek et al., 2020; Morrison et al., 2020; Conroy and Lev, 2020; Chevrel et al., 2018; Castruccio et al., 2010; Pioli et al., 2008; Harris and Allen III, 2008; Harris and Rowland, 2001; Smith, 1997; Dragoni and Tallarico, 1994). Further, constraining crystallinity of igneous rocks is an important component of understanding the petrogenesis of undersampled systems, such as non-terrestrial lava flow fields. The spectral techniques presented here have been used quite extensively in orbital remote sensing and robotic exploration of planetary surfaces and thus much of the work conducted is in that context.

1.2. Spectral capabilities for detecting crystallinity

VNIR spectroscopic analyses of igneous rocks with variable glass content by Cloutis et al. (1990) observed that reflectance from 300 to 2500 nm decreased with increasing glass content. Further, they observed that the samples with lower glass contents and higher crystallinity of minerals exhibited increased spectral reflectance and deeper mineral bands. Similar trends were observed by Minitti et al. (2002) who evaluated the degree of crystallization of synthetic basaltic glass samples, although the spectral brightness was not a focus of that study. Evaluation of their data indicates that the spectral reflectance increased in general from about 300 to 1500 or 2000 nm as the degree of crystallization increased (see for example Fig. 7 in Minitti et al., 2002). The presence of pyroxene bands in the 1800 to 2500 nm region added complexity to the assessment of the reflectance at this wavelength region. An increase in spectral slope from 300 to 2500 nm (red-sloped continuum) has been observed for glassy samples in several studies on crushed samples (Cloutis et al., 1990; Minitti et al., 2002; Carli et al., 2016; Farrand et al., 2016) and this slope increases for fine particle sizes of glass samples (e.g. Minitti et al., 2002). This red-slope in spectra of lunar impact glasses has been associated with impact melt on the Moon (Tompkins and Pieters, 2010), but in this study reflectance did not correlate well with glass content due to highly variable glass compositions. Thus, it appears that VNIR spectral brightness is associated with glass content for basaltic glasses when chemical composition does not vary greatly.

VNIR reflectance spectra of Fe-bearing glasses contain a band near 1000 nm that varies with Fe content and can be distinguished from Fe bands in other minerals (e.g., Adams and McCord, 1971; Burns, 1993; Minitti et al., 2001; Tompkins and Pieters, 2010; Carli et al., 2016); however, identifying glass by this feature in mixtures is difficult because the Fe band in glass spectra occurs near 1100–1200 nm, which overlaps with the broad olivine band (Burns, 1993, Bishop et al., 1993) and the Fe-bearing plagioclase feldspar band near 1250 nm (Adams and Goullaud, 1978). The position and shape of the 1 μm band can be used to identify Fe-bearing glass in VNIR spectra when compositional information is available from other techniques as well (e.g., Horgan and Bell, 2012; Scudder et al., 2021; Henderson et al., 2021).

VNIR reflectance measurements provide a simple, widespread method to analyze rocks in the field, and previous laboratory studies on basalt particles have shown that VNIR spectroscopy can be used to indicate glassiness of volcanic rocks, despite the non-linearity of the relationship between absorption and crystal content (e.g., Hunt et al., 1974; Adams et al., 1974; Dyar and Consolmagno, 1982; Cloutis et al., 1990; Crisp et al., 1990; Minitti et al., 2002; Pompilio et al., 2007; Minitti and Hamilton, 2010; Horgan et al., 2014; Carli et al., 2015; Carli et al., 2016; Farrand et al., 2016; Scudder et al., 2021). Linear unmixing can also be applied using least squares analysis with spectral endmembers (e.g. Adams and Gillespie, 2006; Farrand et al., 2020). However, these studies note that overlap of absorption bands makes precise petrologic analysis challenging. Nevertheless, abundances of mineral phases can be evaluated through spectral unmixing, a more complex modeling method that uses principal component analysis to coordinate the proportion of endmember spectra to the pattern observed in a sample (Keshava and Mustard, 2002). This technique is useful for modeling percentages of all endmember phases, but requires fairly extensive calculations, a thorough knowledge of spectral endmembers, and confidence in the assumptions that go into the model (e.g. Horgan et al., 2017; Cannon et al., 2017).

We extend these studies by investigating the relationship between VNIR spectra and crystallinity in well-characterized basaltic rocks. Although glass content has long been known to lower the overall VNIR reflectance due to glass having very weak spectral absorption bands (e.g., Cloutis et al., 1990; Minitti et al., 2002), this concept has not previously been tested on solid surfaces of natural lavas. Our study is designed to fill this knowledge gap. We selected five basaltic flows to investigate the influence of crystallinity versus glass content on the VNIR reflectance from 500 to 1000 nm of sample surfaces for comparison with planetary surfaces viewed from orbit or from a rover. We acknowledge that a number of factors influence VNIR reflectance in addition to glass content, including mineralogic composition and surface roughness, and for this reason we characterized our samples in detail. We conducted scanning electron microscope (SEM) analyses on young (<10,000 years), unaltered, and uncrushed basalt to identify the dominant mineral assemblages and quantify glass content. These crystallinity estimates from SEM were compared with the VNIR spectral properties in order to test our hypothesis that the magnitude of the reflectance could be used as an indicator for the microcrystallinity in the rock for basaltic lavas.

2. Materials and methods

2.1. Baseline site selection

To ensure a diverse range of petrologic textures common with distributed basaltic volcanism, five field sites were sampled in a transect across the desert region of the western interior of the United States including Hells Half Acre and the Blue Dragon flow in Idaho, Diamond Craters and Devils Garden and Four Craters in Oregon (Fig. 1). These sites were chosen because of their relatively young age (<10,000 bp), basaltic composition (<52 wt% SiO_2 and $Na_2O + K_2O < 5$ wt% whole rock analysis), and low degree of alteration because of the dry climate. Furthermore, there is little morphological evidence for lava/water or ice interactions such as rootless cones, maars, tuff rings, pillow basalts, or lava flows interacting with extensive fluvial networks. This suggests these data can provide a good baseline for low-water emplacement despite there being no record of the precipitation or moisture levels at the time of eruption of these multi-thousand year old flows. The selection of these sites was guided by the desire to minimize factors that confound VNIR reflectance (such as widely varying iron and silica contents, alteration, and dust contamination), while providing a wide variety of natural surfaces (ropey/spiney/shelly pahoehoe, vesicle content) and glass contents that would be expected on basaltic lava flow fields. In this first study, we did not investigate the impact of widely varying bulk chemistry, trace element chemistry, very rough surfaces (such as 'a'a), or lava-derived sediment. These are future directions that will be investigated.

Smooth (2–8 mm roughness), dust-free, intact lava flow surfaces were selected to optimize the quality of the basaltic spectrum. We targeted a range of natural surfaces without regard for crystal content since that could only be determined after sample selection and instead prioritized a variety of emplacement environments, eruption centers, and surface textures within the category of young basalts to ensure natural variability would be accounted for in our dataset. To obtain a full range of crystallinity and glass abundances, we utilized data from previously published holocrystalline basalts and synthetic basaltic glass

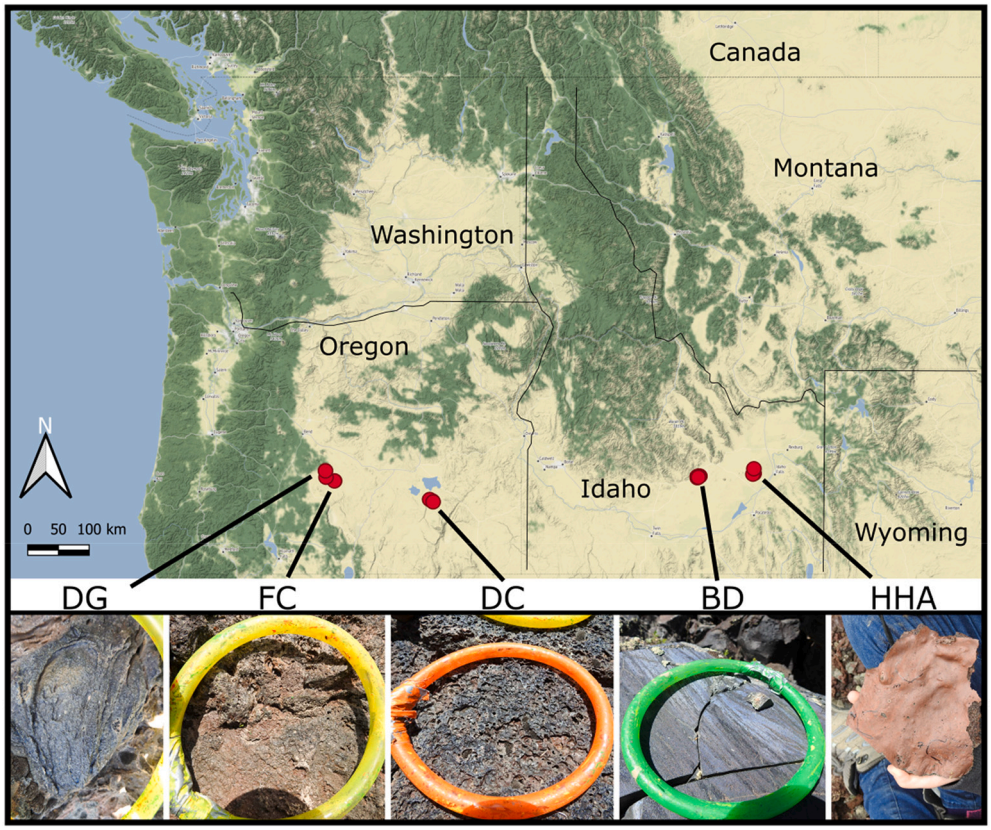

Fig. 1. Map showing field locations and images of analyzed lava flow surfaces from each site. Surfaces varied widely in texture and colour on the millimeter scale. Location names are DG = Devils Garden, FC = Four Craters, DC = Diamond Craters, BD = Blue Dragon, HHA = Hell's Half Acre. (For interpretation of the references to colour in this figure legend, the reader is referred to the web version of this article.)

samples. This is discussed further in section 2.5 below.

2.2. Spectral measurements

Measurements were collected in-situ in the field and in a more controlled laboratory setting with an ASD TerraSpec® Halo portable mineral identifier. This instrument captures continuous single reflectance spectra in the visible near-infrared (extended visible: ~350–1000 nm) and near-infrared (NIR: ~1000–2500 nm) ranges. Samples are illuminated with an internal Quartz Tungsten Halogen bulb with a spot size of ~18 mm while the instrument is in contact with the sample. The spectral resolution is 3 nm for wavelengths 350–700 nm, 9.8 nm for 700–1400 nm, and 8.1 nm for 1400–2100 nm. Each measurement is comprised of 100 spectra averaged over ~20 s. Reflectance spectra are measured relative to Spectralon and corrected for Spectralon absorption irregularities as well as detector offsets (see Sehlke et al., 2019 for details). In the field, the flattest most unaltered exterior was chosen for analysis, and the spectrometer was not moved between triplicate measurements. For laboratory data, the same spot was used, however, the instrument was rotated ~70° to capture the range of readings that could result from a random orientation of the sample in the field due to uneven surfaces (i.e., vesicles, surface flow textures). Three measurements without rotating the sample returned nearly identical spectra, ensuring no instrumental drift or time-dependent variations. The maximum standard deviation between all laboratory readings represents the 1σ uncertainty reported for each sample.

2.3. Petrographic analysis

After in situ analysis, a hand sample of the surface was collected and processed into a thin section for petrographic analysis. The rock was cut with a water saw perpendicular to the analyzed surface and a thin wafer was polished using standard methodology to a 30 μm thickness. This mounting procedure ensures that the thin section provides the same surface measured by the VNIR spectrometer in the field. Between eight and ten SEM images of the upper surface of each sample were collected to ensure a representative calculation (Suppplemental material). Two SEM instruments were used including a Zeiss Supra 35 Variable-Pressure FEG at the University of Idaho and a Hitatchi TM 3000 desktop scanning electron microscope (SEM) with Bruker Q70+ silicon drift detector energy dispersive spectrometer (EDS) system at the APL Space Department SRE meteorite lab. Back Scattered Electron (BSE) images were taken at a working distance of 13–15 mm, with an acceleration voltage of 15–20.00 kV and a magnification of 100× to 300× depending on complexity of mineralogical texture. Elemental maps of Ca, Mg, Fe, Na, Al, and P were produced by scanning the rims using the BSE data for 30 min (Zeiss Supra) or 400 s (Hitachi) at high resolution to assist in mineral identification and quantification. The BSE images are used to calculate the modal abundance via pixel counting of the specific grey scales corresponding to the present phases in the sample (e.g., olivine, pyroxene, feldspar, oxides, and glass) by image processing software. Only a 50 μm band along the top surface was measured as the penetrating depth of VNIR spectroscopy is typically <1.5 μm for opaque samples (Boesche et al., 2015). Error estimates for the modal percentages were calculated using the percentage of variability between five counts of the same sample conducted by five different people. The modal percentage varied by a 1σ standard deviation of 7% of the total crystal content, 5% for olivine and plagioclase, and < 1% for vesicles and oxides.

2.4. Spectral analysis

The magnitude of reflectance between 500 and 1000 nm (abbreviated as $R_{500–1000}$) was calculated by averaging the values between 500 and 1000 nm for a single spectrum, thus quantifying the reflectance of a sample (Fig. 2). The spectra between 350 and 500 were very noisy and thus were excluded from the calculation. We also excluded the portion of the spectra more affected by alteration products (>1000 nm).

2.5. Endmember samples

Finding holocrystalline and crystal-free basaltic glass in the same flow in nature in a high enough quantity to be analyzed by the 1 cm diameter window of the VNIR spectrometer is challenging. Thus, we used synthetically prepared samples including two basaltic samples fused at the Syracuse Lava Project (Rader et al., 2020) and a Shergotitic composition (Sehlke et al., 2020) for glass endmembers. For crystalline endmembers, we chose two natural basalts, one from the Columbia River Flood Basalt province on the Lewiston, ID grade and another from Payun Matru, Argentina (Carli and Sgavetti, 2011). Since most spectra published have been measured of crushed and sieved samples, few spectra in the literature are directly comparable to our data. These samples were all measured as either a rough-cut surface or natural surface, similar to our data set of natural lava samples.

3. Results

3.1. Petrology

The petrology of our samples varies sufficiently in feldspar, olivine, and alteration to test these parameters in comparison with the spectral properties. The 2-D percentage of glass in the 17 samples ranged from 27 to 83% (Table 1). All samples contained plagioclase (11–56%) and vesicles (0.5–17%). All but one sample contained olivine (1–16%) and nine samples contained Fe-oxides (0.1–9.1%). Three samples contained small amounts of apatite (0.2–0.6%). Samples were categorized by the abundance of mineral phases in the order of iron oxide, olivine, and then plagioclase in the following decision tree
.

3.2. Spectral classification

Spectral absorption bands are present at a combination of wavelengths that are indicative of primary minerals and phases (e.g., feldspar, iron-oxides), as well as clay minerals produced by chemical weathering and lichen (Salehi et al., 2017, Fig. 2). Despite olivine phenocrysts being present in all but one sample, olivine signatures were not strong in the spectra, which is consistent with other findings that olivine is typically difficult to detect at abundances below ~20–25% in mixtures (e.g., Singer, 1981; Cloutis et al., 1986; Parente et al., 2011).

Reflectance values, which were averaged over the spectral range 500–1000 nm, varied from 0.039 to 0.136 (field) and 0.049 to 0.127 (lab) with most spectra having a maximum standard deviation of <1% between replicates ($n = 9$). Four spectra had an error of <10%, three with <15%, one with an error of 20%, and one with an error of 57% within the triplicate set. The largest variability was found for the laboratory measurements when samples were rotated and represent the maximum variation possible, which is reported in Table 1. This may have been due to an increase in specular reflectance when rotating some of the glassy samples. Most samples ($n = 14$) have reflectance values between 0.04 and 0.1 over the entire range of wavelengths in both laboratory and field spectra, however, reflectance values tended to be higher in the laboratory analyses (Fig. 3). Glassier samples also tended to have lower reflectance and contain fewer spectral features compared to more crystalline samples.

4. Discussion

4.1. Effects of glass content on the $R_{500–1000}$ value of whole rock surfaces

Unlike previous studies on powdered samples, rock surface analyses do not exhibit the spectral feature associated with mafic glass, a broad

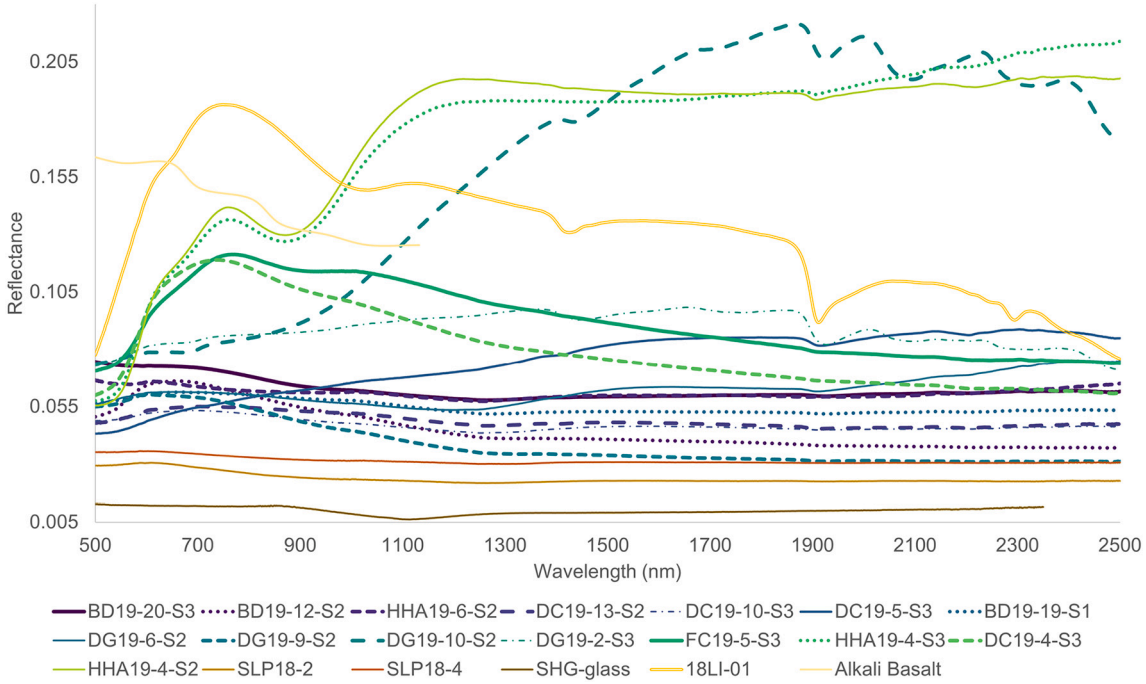

Fig. 2. Average lab and field spectra for the 16 natural samples included in Fig. 4 as well as the endmember spectra in brown and yellow colors. Colour corresponds to the vol% of glass in the sample with darker purple = more glass, fewer crystals, lighter green = less glass and more crystals. (For interpretation of the references to colour in this figure legend, the reader is referred to the web version of this article.)

Table 1
Summary of VNIR and phases of the averaged spectra for each sample. Alkali basalt endmember spectra from Carli and Sgavetti (2011).

	Modal abundance of phases (%)								$R_{500–1000}$				
Sample name	Plagioclase	Olivine	Glass	Vesicles	Oxides	Apatite	% Crystal	1s	Field	Lab	Average	Max s	Category
BD19–12-S2	11	1.6	78	7.9	0.6	0.2	22	2	0.056	0.062	0.059	0.0003	glass
BD19–20-S3	14	2.4	82	1.5	1.6	0.4	18	2	0.062	0.076	0.069	0.003	glass
BD19–19-S1	15	4.6	69	7.9	2.5	0.6	31	3	0.064	0.055	0.059	0.0002	glass
DC19–11-S3	16	0.7	83	0.5	0	0	17	2	0.054	0.065	0.059	0.006	glass
HHA19–6-S2	16	2.8	76	5.1	0	0	24	2	0.072	0.054	0.063	0.01	glass
FC19–5-S3	27	6.5	49	17	0	0	51	5	0.088	0.125	0.107	0.0009	olivine
DG19–10-S2	31	8.8	58	1.3	0.4	0	42	4	0.075	0.094	0.085	0.0006	olivine
DG19–2-S3	36	5.6	56	2.1	0	0	44	4	0.061	0.108	0.084	0.03	olivine
DC19–4-S3	46	9.2	38	6.7	0	0	62	6	0.105	0.101	0.103	0.008	olivine
DG19–11-S3	49	16	34	0.5	0.5	0	66	7	0.115	–	0.115	0.006	olivine
HHA19–4-S3	42	8.0	39	2.1	8.6	0	61	6	0.136	0.097	0.117	0.0007	oxide
HHA19–4-S2	56	2.6	27	5.2	9.1	0	73	7	0.106	0.127	0.117	0.001	oxide
DC19–10-S3	20	3.8	71	5.0	0.1	0	29	3	0.052	0.049	0.051	0.0002	plagioclase
DC19–13-S2	21	2.6	74	2.2	0	0	26	3	0.057	0.049	0.053	0.0004	plagioclase
DC19–5-S3	21	0	71	8.3	0	0	29	3	0.056	0.055	0.056	0.0003	plagioclase
DG19–6-S2	23	3.2	68	5.2	0.1	0	32	3	0.057	0.062	0.059	0.0003	plagioclase
DG19–9-S2	26	2.5	58	14	0	0	42	4	0.039	0.070	0.054	0.006	plagioclase
Alkali Basalt	–	–	0	–	–	–	100	0	–	0.143	–	–	crystalline endmember
18LI-01	–	–	0	–	–	–	100	0	0.159	–	–	0.008	crystalline endmember
SLP18–02	0	0	100	0	0	0	0	0	–	0.027	–	–	glass endmember
SLP18–04	0	0	100	0	0	0	0	0	–	0.034	–	–	glass endmember
SHG-glass	0	0	100	0	0	0	0	0	–	0.013	–	0.0007	glass endmember

Data summary showing the modal abundance of each phase identified in each sample, the $R_{500–1000}$ value of field, lab, and average VNIR data, and the spectral classification.

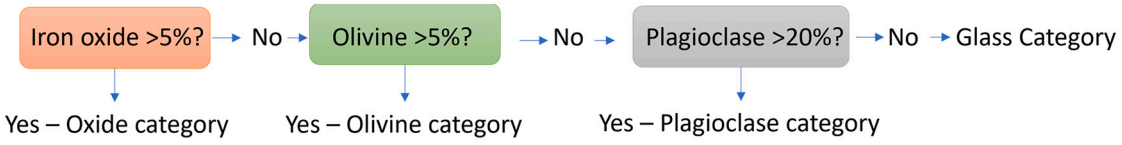

absorption band between the wavelengths of 1.08–1.18 μm (Carli et al., 2015). Instead, we found absorption bands at wavelengths characteristic of the observed primary minerals (except for olivine) and increased $R_{500–1000}$ values with increasing crystallinity (Pearson correlation coefficient of 0.7). The mineralogy of a fresh basalt is fairly limited to olivine, plagioclase, Fe-oxides, and occasionally pyroxene, making the spectral classification simple enough to use the $R_{500–1000}$ value as a proxy for glass content. However, this trend may not hold for all lava compositions or mineralogies. Several samples in our data set also included minor amounts of apatite, which did not affect the relationship between crystallinity and $R_{500–1000}$. Based on these results, glassier basalts have lower reflectance from 500 to 1000 nm relative to more crystalline basalts.

To estimate crystal content, we assumed a linear relationship between modal crystal content and the $R_{500–1000}$ value (Table 1). The following equation allows for the prediction of the crystallinity/glassiness of basaltic samples as a function of reflectance at 500–1000 nm with a 8.4 vol% standard error at the 95% confidence level:

$$Vol\%Crystal = -16.1(\pm 4.1) + (725(\pm 49) * R_{500-1000})$$

Errors on parameters for this linear relationship (r^2 of 0.92) are given in parentheses. Exceptions include samples with very rough surfaces, which in contact probes can cause protrusions to be closer to the detector and appear brighter than other samples with a different crystallinity. On the other hand, "spectral darkening" (lower reflectance) may be a consequence of the formation of a fragile thin layer of glazed glass. This layer can be lost during sample preparation (evidence for this in our samples was seen as cracked and missing glassy rinds in SEM imagery) leading to crystallinities that appear higher than what the spectrometer originally detected, as the outer layer was primarily glass when first analyzed. Differences in $R_{500–1000}$ between the rough and glazed samples due to crystalline components may be up to 20% and likely constitutes the majority of the variability between modeled and actual glass abundance and warrants further study (Fig. 4). Despite having the ability to shift $R_{500–1000}$, glass content played a stronger role than surface characteristics for the majority of the natural samples, suggesting this method is robust enough to overcome the natural variablility that occurs in basaltic lava flow fields.

4.2. *Ideal wavelengths for crystallinity proxy*

Whereas reflectance tends to increase with crystal content over a wide range of wavelengths, we chose to use the range of 500–1000 nm because this range encompasses most of the absorptions related to the primary mineralogy common in basalts (olivine, glass, clinopyroxene, plagioclase, Fe oxides), while excluding effects of alteration and lichen seen at longer wavelengths. Beginning at 500 nm also has the advantage of excluding any variation at shorter wavelengths due to standard calibration, lighting, scattering, or instrument effects. Altered samples exhibiting more prominent hydration bands also tended to have higher reflectance between 1100 and 2500 nm, which could skew an average of the reflectance that includes these higher wavelengths. Including reflectance values in this longer wavelength range causes a disjointed dataset instead of a more linear relationship and thus we chose to exclude higher values from our calculation. However, we tested selected reflectance values at specific wavelengths to determine if the observed trends still hold. The reflectance of single values at 700, 1200, and 1700 nm, were evaluated for a subset of the data and show the same correlation observed for the reflectance across the range 500–1000 nm, although the slope of the best fit line shifts slightly (Supplemental material). Similarly, a spectrometer in a controlled lab setting with improved stability at lower wavelengths may provide suitable data

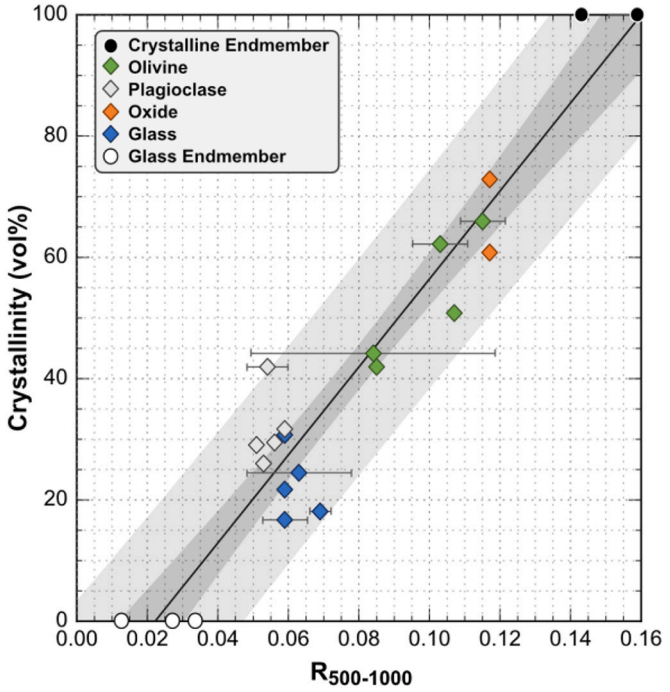

Fig. 3. Crystal abundance determined by SEM images compared to the $R_{500–1000}$ value. The inner shaded region is the region of correlation that would match the data set at a 95% confidence level. The outer shaded region is the region of likelihood at a 95% confidence that would contain any future data points. Symbol colour indicates the mineral characterization. Blue is glass, grey is plagioclase, orange is oxide, green is olivine, black is crystalline endmembers and white is glass endmembers. The variance bars for some samples are less than the size of the symbol. (For interpretation of the references to colour in this figure legend, the reader is referred to the web version of this article.)

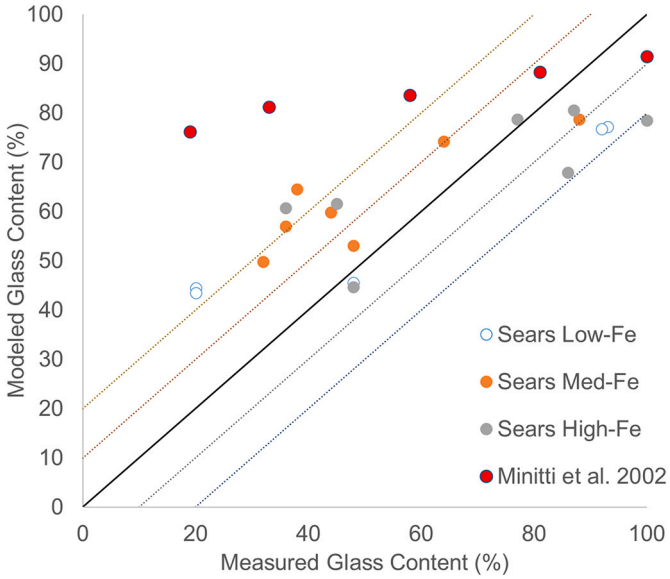

Fig. 4. Modeled versus measured glass content of three data sets. Broken surfaces of basalt samples published in Sears et al., 2017 are organized by iron content (white, orange, grey). Ground and sieved synthetic basalt published in Minitti et al., 2002 is shown in red. Lines indicate the 0%, 10%, and 20% error envelope. (For interpretation of the references to colour in this figure legend, the reader is referred to the web version of this article.)

down to 300 nm. Different planetary atmospheres may have different spectral windows and thus, this method can be adapted to the wavelengths that are optimal for a given planetary body. Similarly, if absolute reflectance can not be obtained, a comparison of the relative reflectance of different outcrops may allow for relative crystallinity within a flow or region of flows.

4.3. Comparison to crushed, sieved, or broken interior samples

The method of in-situ natural surface measurements differs greatly from the standard VNIR spectral collection which typically includes crushing and sieving samples. Changing the particle size of a granular sample affects the $R_{500–1000}$ value with smaller particle sizes increasing both the reflectance and the strength of absorption bands (Carli et al., 2016). Similarly, crushing and sieving a sample, or using synthetic material with no vesicles removes the variability due to surface roughness (Leight, 2020). Thus, we cannot directly compare absolute values or slopes of datasets collected in different ways, however, we observe that overall reflectance does increase with increasing crystallinity (Fig. 5). Synthetic glass and crystalline mixtures of basaltic compositions crushed and sieved to 75–500 μm published by Minitti et al. (2002) shows a very clean trend ($r^2 = 0.97$) with a lower slope than the natural data. Similarly, the positive correlation between $R_{500–1000}$ and crystallinity is visible ($r^2 = 0.74$) in a series of 19 basalt samples published by Sears et al. (2017) however the slope is slightly shallower than our data. The Sears et al. samples were collected for geochemistry purposes and thus contained only broken surfaces of clean interior lava flows which were less rough than the natural surfaces. To ensure accurate modeled crystal abundances, samples should be analyzed on the same type of surface as the data used to create the relationship, be it crushed and sieved, broken or cut surface, or a natural surface of similar roughness. Thus, for analyses of lava flows, using natural lava surfaces provides the best analog.

4.4. Implications for interpreting ancient eruptions on earth and other planets

The purpose of this study was to determine if data collected in a similar way to field measurements with a contact VNIR probe and natural lava flow surfaces would show a clear relationship between $R_{500–1000}$ and glass/crystal content. Whereas laboratory studies on

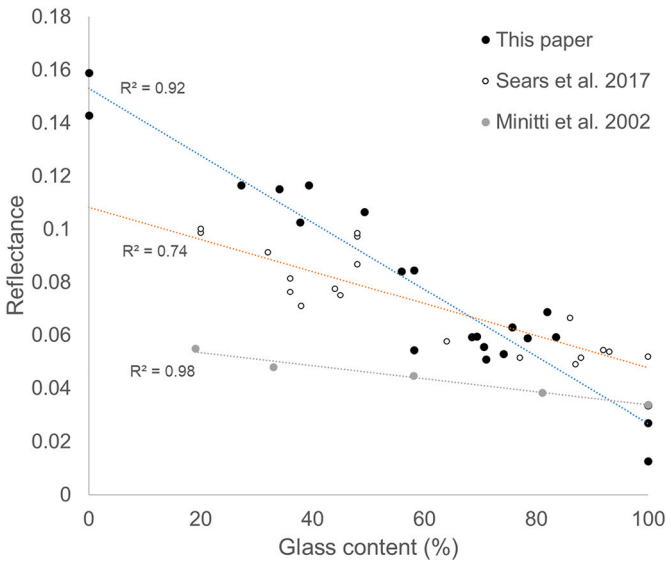

Fig. 5. Glass content compared to overall reflectance between 500 and 1000 nm of comparison datasets. Data from this paper (black dots) show a steeper trend than data collected on smoother surfaces (Sears et al., 2017 in white) or crushed and sieved samples (Minitti et al., 2002 in grey).

prepared and sieved samples result in a more tight relationship, it also increases the time and cost of analysis. This method could be employed immediately to start estimating glass contents of basalt surfaces of similar roughness in field settings without collecting samples for analysis. This has practical applications in volcanology and planetary science because of the role that cooling rate has on glass abundances.

Natural surfaces may be altered in numerous ways which may affect the basic relationship between $R_{500–1000}$ and crystallinity. However, surfaces cleared of dust/regolith by wind, or a rover, or flow surfaces exposed inside of lava tubes or in crater rims, or extremely young flows such as those on Io would be prime candidates for this type of analysis. If clean or fresh surfaces are exposed, this technique could inform geologic processes that lead to high or low contents of glass and crystalline minerals. For example, a lava flow's cooling rate dictates the abundance of glass and thus several analyses from a flow field may indicate the presence of water in the environment in which the lava was emplaced (Wall et al., 2014; Mastin, 2007; Gregg and Fornari, 1998; Keszthelyi and Denlinger, 1996). Thus, lava that interacted with water or ice would cool faster and have fewer crystalline minerals. These water/ice-triggered rapid cooling events may be evident from low spectral reflectance values. Further work on flow fields with documented water-lava interactions is planned. Additionally, further work on differing tectonic settings such as hotspot volcanism (including Iceland and Hawaii), as well as subduction-related basalts found in the Cascade arc may enable extrapolation of these results to a wider range of lava types. However, the differences in chemistry between these settings (predominantly trace elements) are unlikely to influence the reflectance value over the range 500–1000 nm and thus we believe these results can be more widely applied to other basaltic systems.

Broad crystallinity estimates of lava flows could also provide insight into magma generation, storage, transport, and eruption dynamics in unsampled volcanic systems all across planetary surfaces (e.g. Marsh, 1981; Cashman and McConnell, 2005; Woitischek et al., 2020). While crystallinity may be measured through direct sampling using other systems on the Martian rovers currently, they require sample preparation that takes time and energy. This novel method of estimating crystallinity would be simpler, faster, and require fewer resources.

5. Conclusions

The magnitude of reflectance over the 500–1000 nm spectral range of basaltic lava surfaces is lower for higher glass contents given similar surface roughnesses. This pattern is demonstrated through spectroscopic analyses of 17 samples from five basaltic flow fields in the northwestern USA and compared to two published datasets. Using the $R_{500–1000}$ value, the total crystallinity can be estimated within 8% for most samples, with outliers resulting from sample preparation and surface roughness variability. Similar findings regardling surface roughness of basalt can be found in Sehlke et al. (2019). Smoother or broken surfaces and crushing the sample result in higher overall reflectance for glassier samples. Within the natural variability of basalt flows, iron content does not interfere considerably with this relationship, however it would likely need to be considered when comparing basalts to other lava compositions. Highly vesiculated basalt with phenocrysts and microlites may show spectral absorptions consistent with glass and thus might be misinterpreted as highly glassy without the inclusion of the $R_{500–1000}$ value to approximate the quantity of crystals. The ability to determine the crystallinity of basaltic lava flow surfaces using a handheld VNIR spectrometer would enable the exploration and characterization of larger areas during extravehicular activities of planetary surfaces compared to robotic assets.

Acknowledgments, samples, and data

Thank you to the APL Space Department SRE meteorite lab for the use of the SEM. This research was supported by NASA PSTAR grant #80NSSC18K1518, and a Hill Undergraduate Research Fellowship. Samples from Craters of the Moon National Monument and Preserve were collected under permit #CRMO-2019-SCI-004. Assistance in the field was provided by Adrianne Reeder and Kevin Cerna.

Declaration of Competing Interest

None.

Appendix A. Supplementary data

Supplementary data to this article can be found online at https://doi.org/10.1016/j.icarus.2022.115084.

References

Adams, J.B., Gillespie, A.R., 2006. Remote Sensing of Landscapes with Spectral Images: A Physical Modeling Approach. Cambridge University Press.
Adams, J.B., Goullaud, L.H., 1978. Plagioclase feldspars - visible and near infrared diffuse reflectance spectra as applied to remote sensing. In: Proceedings, 9th Lunar and Planetary Science Conference, pp. 2901–2909.
Adams, J.B., McCord, T.B., 1971. Optical properties of mineral separates, glass, and anorthositic fragments from Apollo mare samples. In: Proceedings of the 2nd Lunar Science Conference, vol. 3, pp. 2183–2195.
Adams, J.B., Pieters, C., McCord, T.B., 1974. Orange glass-evidence for regional deposits of pyroclastic origin on the moon. In: Lunar and Planetary Science Conference Proceedings, vol. 5, pp. 171–186.
Armienti, P., 2008. Decryption of igneous rock textures: crystal size distribution tools. Rev. Mineral. Geochem. 69 (1), 623–649.
Bernard, O., de Maisonneuve, C.B., 2020. Controls on eruption style at Rabaul, Papua New Guinea–Insights from microlites, porosity and permeability measurements. J. Volcanol. Geotherm. Res. 406, 107068.
Biren, J., Harris, A., Tuffen, H., Gurioli, L., Chevrel, M.O., Vlastélic, I., Calabro, L., 2020. Chemical, textural and thermal analyses of local interactions between lava flow and a tree–case study from Pāhoa, Hawai'i. Front. Earth Sci. 8.
Bishop, J.L., Pieters, C.M., Burns, R.G., 1993. Reflectance and Mössbauer spectroscopy of ferrihydrite-montmorillonite assemblages as Mars soil analog materials. Geochim. Cosmochim. Acta 57, 4583–4595.
Boesche, N.K., Rogass, C., Lubitz, C., Brell, M., Herrmann, S., Mielke, C., Kaufmann, H., 2015. Hyperspectral REE (rare earth element) mapping of outcrops—applications for neodymium detection. Remote Sens. 7 (5), 5160–5186.
Burkhard, D.J., 2002. Kinetics of crystallization: example of micro-crystallization in basalt lava. Contrib. Mineral. Petrol. 142 (6), 724–737.
Burns, R.G., 1993. Mineralogical Applications of Crystal Field Theory. Cambridge University Press, Cambridge, UK, p. 551.
Cannon, K.M., Mustard, J.F., Parman, S.W., Sklute, E.C., Dyar, M.D., Cooper, R.F., 2017. Spectral properties of Martian and other planetary glasses and their detection in remotely sensed data. J. Geophys. Res. Planets 122 (1), 249–268.
Carli, C., Sgavetti, M., 2011. Spectral characteristics of rocks: effects of composition and texture and implications for the interpretation of planet surface compositions. Icarus 211 (2), 1034–1048.
Carli, C., Serventi, G., Sgavetti, M., 2015. VNIR spectral characteristics of terrestrial igneous effusive rocks: mineralogical composition and the influence of texture. Geol. Soc. Lond., Spec. Publ. 401 (1), 139–158.
Carli, C., Roush, T.L., Pedrazzi, G., Capaccioni, F., 2016. Visible and near-infrared (VNIR) reflectance spectroscopy of glassy igneous material: spectral variation, retrieving optical constants and particle sizes by Hapke model. Icarus 266, 267–278.
Cashman, K.V., McConnell, S.M., 2005. Multiple levels of magma storage during the 1980 summer eruptions of Mount St. Helens, WA. Bull. Volcanol. 68 (1), 57–75.
Cashman, K.V., Thornber, C., Kauahikaua, J.P., 1999. Cooling and crystallization of lava in open channels, and the transition of Pāhoehoe lava to'A'ā. Bull. Volcanol. 61 (5), 306–323.
Castruccio, A., Rust, A.C., Sparks, R.S.J., 2010. Rheology and flow of crystal-bearing lavas: insights from analogue gravity currents. Earth Planet. Sci. Lett. 297 (3–4), 471–480.
Chevrel, M.O., Harris, A.J., James, M.R., Calabrò, L., Gurioli, L., Pinkerton, H., 2018. The viscosity of pāhoehoe lava: in situ syn-eruptive measurements from Kilauea, Hawaii. Earth Planet. Sci. Lett. 493, 161–171.
Cloutis, E.A., Gaffey, M.J., Jackowski, T., Reed, K., 1986. Calibration of phase abundance, composition, and particle size distribution for olivine-orthopyroxene mixtures from reflectance spectra. J. Geophys. Res. 91, 11641–11653.
Cloutis, E.A., Gaffey, M.J., Smith, D.G., Lambert, R.S.J., 1990. Reflectance spectra of glass-bearing mafic silicate mixtures and spectral deconvolution procedures. Icarus 86 (2), 383–401.
Conroy, C.J., Lev, E., 2020. A discontinuous Galerkin finite element model for fast channelized lava flows v1. 0. Geosci. Model Dev. Discuss. 1–27.
Crisp, J., Kahle, A.B., Abbott, E.A., 1990. Thermal infrared spectral character of Hawaiian basaltic glasses. J. Geophys. Res. Solid Earth 95 (B13), 21657–21669.
DeGraff, J.M., Long, P.E., Aydin, A., 1989. Use of joint-growth directions and rock textures to infer thermal regimes during solidification of basaltic lava flows. J. Volcanol. Geotherm. Res. 38 (3–4), 309–324.

Dragoni, M., Tallarico, A., 1994. The effect of crystallization on the rheology and dynamics of lava flows. J. Volcanol. Geotherm. Res. 59 (3), 241–252.
Dyar, M.D., Consolmagno, G.J., 1982, March. Ferric Iron in lunar glasses and the interpretation of lunar spectra. In: Lunar and Planetary Science Conference, vol. 13, pp. 193–194.
Farrand, W.H., Wright, S.P., Rogers, A.D., Glotch, T.D., 2016. Basaltic glass formed from hydrovolcanism and impact processes: characterization and clues for detection of mode of origin from VNIR through MWIR reflectance and emission spectroscopy. Icarus 275, 16–28.
Farrand, W.H., Merényi, E., Parente, M., 2020. Hyper- and multispectral VNIR imaging analysis. In: Bishop, J., Bell, J.F., Moersch, J. (Eds.), Remote Compositional Analysis: Techniques for Understanding Spectroscopy, Mineralogy, and Geochemistry of Planetary Surfaces, vol. 2019. Cambridge University Press, Cambridge, UK, pp. 307–323.
Gregg, T.K., Fornari, D.J., 1998. Long submarine lava flows: observations and results from numerical modeling. J. Geophys. Res. Solid Earth 103 (B11), 27517–27531.
Griffiths, R.W., 2000. The dynamics of lava flows. Annu. Rev. Fluid Mech. 32 (1), 477–518.
Harris, A.J., Allen III, J.S., 2008. One-, two-and three-phase viscosity treatments for basaltic lava flows. J. Geophys. Res. Solid Earth 113 (B9).
Harris, A.J., Rowland, S., 2001. FLOWGO: a kinematic thermo-rheological model for lava flowing in a channel. Bull. Volcanol. 63 (1), 20–44.
Henderson, M.J.B., Horgan, B.H.N., Rowe, M.C., Wall, K.T., Scudder, N.A., 2021. Determining the volcanic eruption style of tephra deposits from infrared spectroscopy. Earth Space Sci. 8, e2019EA001013.
Horgan, B., Bell, J.F., 2012. Widespread weathered glass on the surface of Mars. Geology. https://doi.org/10.1130/G32755.1.
Horgan, B.H., Cloutis, E.A., Mann, P., Bell III, J.F., 2014. Near-infrared spectra of ferrous mineral mixtures and methods for their identification in planetary surface spectra. Icarus 234, 132–154.
Horgan, B.H., Smith, R.J., Cloutis, E.A., Mann, P., Christensen, P.R., 2017. Acidic weathering of basalt and basaltic glass: 1. Near-infrared spectra, thermal infrared spectra, and implications for Mars. J. Geophys. Res. Planets 122 (1), 172–202.
Hunt, G.R., GR, H., JW, S., CJ, L., 1974. Visible and near Infrared Spectra of Minerals and Rocks. IX. Basic and Ultrabasic Igneous Rocks.
Keshava, N., Mustard, J.F., 2002. Spectral unmixing. IEEE Signal Process. Mag. 19 (1), 44–57.
Keszthelyi, L., Denlinger, R., 1996. The initial cooling of pahoehoe flow lobes. Bull. Volcanol. 58 (1), 5–18.
Leight, C., 2020. Characterizing Volcaniclastic Deposits on Planetary Surfaces Using Remote Sensing Observations.
Marsh, B.D., 1981. On the crystallinity, probability of occurrence, and rheology of lava and magma. Contrib. Mineral. Petrol. 78 (1), 85–98.
Mastin, L.G., 2007. Generation of fine hydromagmatic ash by growth and disintegration of glassy rinds. J. Geophys. Res. Solid Earth 112 (B2).
McBride, M.J., Bennett, K.A., Gaddis, L.R., Horgan, B.H.N., Glaspie, L.M., 2019. Volcanic glass distribution and potential source vents for the Taurus-Littrow pyroclastic deposit at the Apollo 17 landing site region. LPI 2132, 3039.
Minitti, M.E., Hamilton, V.E., 2010. A search for basaltic-to-intermediate glasses on Mars: assessing martian crustal mineralogy. Icarus 210 (1), 135–149.
Minitti, M.E., Mustard, J.F., Rutherford, M.J., 2001. The effects of glass content and oxidation on the spectra of SNC-like basalts: application to Mars remote sensing. J. Geophys. Res. Planets 1–55.
Minitti, M.E., Mustard, J.F., Rutherford, M.J., 2002. Effects of glass content and oxidation on the spectra of SNC-like basalts: applications to Mars remote sensing. J. Geophys. Res. Planets 107 (E5), 6-1.
Morrison, A.A., Whittington, A., Smets, B., Kervyn, M., Sehlke, A., 2020. The rheology of crystallizing basaltic lavas from Nyiragongo and Nyamuragira volcanoes, DRC. Volcanica 3 (1), 1–28.
Parente, M., Makarewicz, H.D., Bishop, J.L., 2011. Decomposition of mineral absorption bands using nonlinear least squares curve fitting: application to Martian meteorites and CRISM data. Planet. Space Sci. 59, 423–442.
Pioli, L., Erlund, E., Johnson, E., Cashman, K., Wallace, P., Rosi, M., Granados, H.D., 2008. Explosive dynamics of violent Strombolian eruptions: the eruption of Parícutin volcano 1943–1952 (Mexico). Earth Planet. Sci. Lett. 271 (1–4), 359–368.
Pompilio, L., Sgavetti, M., Pedrazzi, G., 2007. Visible and near-infrared reflectance spectroscopy of pyroxene-bearing rocks: new constraints for understanding planetary surface compositions. J. Geophys. Res. Planets 112 (E1).
Pupier, E., Duchene, S., Toplis, M.J., 2008. Experimental quantification of plagioclase crystal size distribution during cooling of a basaltic liquid. Contrib. Mineral. Petrol. 155 (5), 555–570.
Rader, E., Wysocki, R.S., Heldmann, J., Harpp, K., Bosselait, M., Myers, M., 2020. Spatter stability: constraining accumulation rates and temperature conditions with experimental bomb morphology. Bull. Volcanol. 82, 1–18.
Robert, B., Harris, A., Gurioli, L., Médard, E., Sehlke, A., Whittington, A., 2014. Textural and rheological evolution of basalt flowing down a lava channel. Bull. Volcanol. 76 (6), 1–21.
Salehi, S., Rogge, D., Rivard, B., Heincke, B.H., Fensholt, R., 2017. Modeling and assessment of wavelength displacements of characteristic absorption features of common rock forming minerals encrusted by lichens. Remote Sens. Environ. 199, 78–92.
Scudder, N.A., Horgan, B.H., Rampe, E.B., Smith, R.J., Rutledge, A.M., 2021. The effects of magmatic evolution, crystallinity, and microtexture on the visible/near-infrared and thermal-infrared spectra of volcanic rocks. Icarus 114344.
Sears, D.W., Sears, H., Sehlke, A., Hughes, S.S., 2017. Induced thermoluminescence as a method for dating recent volcanism: eastern Snake River plain, Idaho, USA. J. Geophys. Res. Solid Earth 122 (2), 906–922.
Sehlke, A., Mirmalek, Z., Burtt, D., Haberle, C.W., Santiago-Materese, D., Kobs Nawotniak, S.E., Lim, D.S., 2019. Requirements for portable instrument suites during human scientific exploration of Mars. Astrobiology 19 (3), 401–425.
Sehlke, A., Hofmeister, A.M., Whittington, A.G., 2020. Thermal properties of glassy and molten planetary candidate lavas. Planet. Space Sci. 193, 105089 https://doi.org/10.1016/J.PSS.2020.105089.
Singer, R.B., 1981. Near-infrared spectral reflectance of mineral mixtures: systematic combinations of pyroxenes, olivine, and iron oxides. J. Geophys. Res. 86, 7967–7982.
Smith, J.V., 1997. Shear thickening dilatancy in crystal-rich flows. J. Volcanol. Geotherm. Res. 79 (1–2), 1–8.
Tompkins, S., Pieters, C.M., 2010. Spectral characteristics of lunar impact melts and inferred minerology. Meteorit. Planet. Sci. 45, 1152–1169.
Wall, K.T., Rowe, M.C., Ellis, B.S., Schmidt, M.E., Eccles, J.D., 2014. Determining volcanic eruption styles on earth and Mars from crystallinity measurements. Nat. Commun. 5 (1), 1–8.
Woitischek, J., Edmonds, M., Woods, A.W., 2020. The control of magma crystallinity on the fluctuations in gas composition at open vent basaltic volcanoes. Sci. Rep. 10 (1), 1–7.